AGU PUBLICATIONS

JGR

Journal of Geophysical Research: Solid Earth

RESEARCH ARTICLE
10.1002/2014JB011619

Key Points:
- A model for free convection steam condensation heat transfer is developed
- Heat transfer rates may be further increased by forced convection
- Heat fluxes approach those inferred from recent volcanic eruptions

Supporting Information:
- Text S1
- Model S1

Correspondence to:
D. C. Woodcock,
d.woodcock@lancaster.ac.uk

Citation:
Woodcock, D. C., J. S. Gilbert, and S. J. Lane (2015), Ice-melt rates by steam condensation during explosive subglacial eruptions, *J. Geophys. Res. Solid Earth*, *120*, 864–878, doi:10.1002/2014JB011619.

Received 18 SEP 2014
Accepted 11 JAN 2015
Accepted article online 14 JAN 2015
Published online 11 FEB 2015

Ice-melt rates by steam condensation during explosive subglacial eruptions

D. C. Woodcock[1], J. S. Gilbert[1], and S. J. Lane[1]

[1]Lancaster Environment Centre, Lancaster University, Lancaster, UK

Abstract Subglacial volcanism melts cavities in the overlying ice. These cavities may be flooded with meltwater or they may be fully or partially drained. We quantify, for the first time, heat transfer rates by condensation of steam on the walls and roof of a fully or partially drained subglacial eruption cavity. Our calculations indicate that heat fluxes of up to 1 MW m^{-2} may be obtained when the bulk vapor in the cavity is in free convection. This is considerably smaller than heat fluxes inferred from ice penetration rates in recent subglacial eruptions. Forcing of the convection by momentum transfer from an eruption jet may allow heat fluxes of up to 2 MW m^{-2}, consistent with values inferred for the Gjálp 1996 subglacial eruption. Vapor-dominated cavities in which vapor-liquid equilibrium is maintained have thermal dynamic responses that are an order of magnitude faster than the equivalent flooded cavities.

1. Introduction

Subglacial volcanism melts cavities in the overlying ice. In most cases the resulting meltwater drains from the eruption site to be released at the ice margin as a jökulhlaup or to be stored in a subglacial lake [*Gudmundsson et al*., 2004; *Magnússon et al*., 2012]. For temperate (wet-based) glaciers, the extent of drainage of the resulting meltwater appears to be determined by subglacial hydrology rather than by volume changes occurring during magma-ice interaction [*Höskuldsson and Sparks*, 1997]. Thus, a cavity may be liquid filled, fully drained, or partly drained. Figure 1 shows a case where a subglacial eruption cavity is partly drained.

Heat transfer during subglacial eruptions has been considered by *Höskuldsson and Sparks* [1997]; *Wilson and Head* [2002, 2007], and *Gudmundsson* [2003]. Figure 11 in *Gudmundsson* [2003] shows a schematic illustration of a liquid-filled (flooded) cavity part way through a subglacial eruption. *Woodcock et al*. [2014] considered heat transfer within such a cavity by single-phase and boiling two-phase free convection. *Tuffen et al*. [2002] discussed the possibility of fully drained cavities in the context of subglacial rhyolitic eruptions.

We use the Gjálp eruption under the Vatnajökull ice cap, Iceland in October 1996 as a benchmark for our calculations because this is one of the best documented examples of a subglacial explosive eruption [*Gudmundsson et al*., 1997, 2004]. This eruption penetrated a thickness of 500–600 m of ice in around 30 h after the start of the eruption. Ice-melting rates of up to 0.5 km^3 per day were inferred by repeated observations of depressions that developed in the ice surface above the eruption site and by changes in the volume of water in the subglacial lake Grimsvötn.

1.1. Scope of Paper

If an ice cavity is fully or partially drained, rather than flooded, heat may be transferred from magma to ice via steam generation and condensation. For the fully drained case we envisage a predominantly steam-filled cavity within which a limited inventory of water repeatedly boils (by contact with magma) and condenses on the roof and walls of the ice cavity. Although drained of meltwater, the cavity is deluged by an intense shower of meltwater and steam condensate from the cavity roof. There should thus be sufficient liquid water available to promote phreatomagmatic fragmentation.

The possibility of heat transfer to ice by steam in subglacial eruption cavities has been discussed qualitatively in the literature [*Smellie*, 2002; *Tuffen et al*., 2002]. In this paper we quantify (1) heat transfer rates from steam condensation on the ice cavity surface, using published heat transfer methods to estimate likely heat fluxes, (2) the thermal dynamic response of a vapor-dominated cavity to a change in heat input, and (3) the conditions under which a fully or partially drained subglacial cavity may exist.

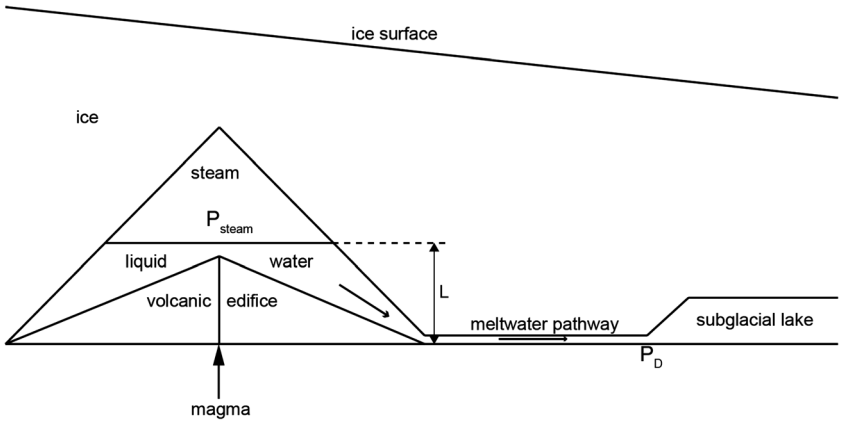

Figure 1. Schematic diagram of a partly drained subglacial eruption cavity that drains meltwater into a subglacial lake.

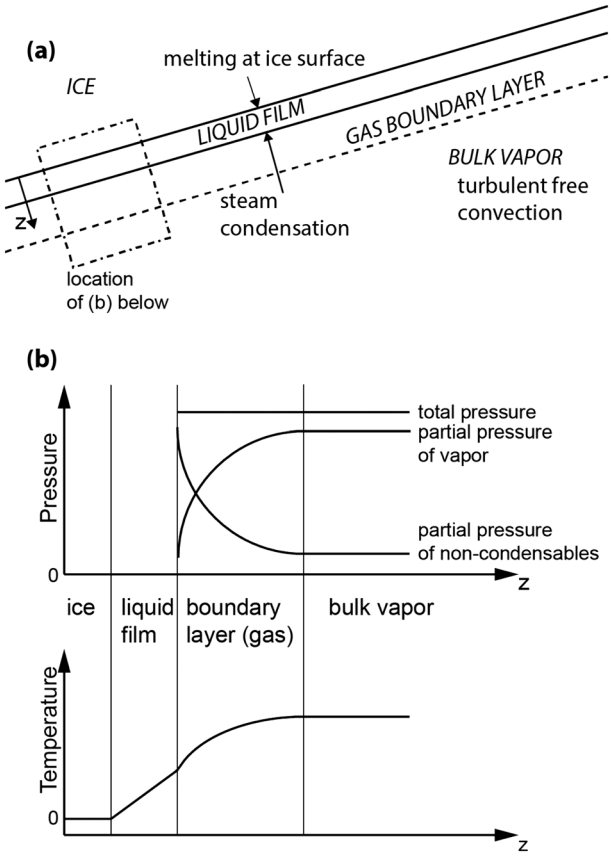

Figure 2. **(a)** Summary of various aspects of heat transfer on the sloping wall of a drained but steam-filled ice cavity. Heat is transferred from the cavity bulk vapor to the ice surface through two thermal resistances in series: a gas boundary layer and a liquid film. **(b)** The influence of noncondensables on interfacial resistance. The partial pressures of vapor and of noncondensables in the bulk and their variation through the gas-vapor film are shown diagrammatically (the ice surface is vertical for ease of comprehension). The corresponding variation in vapor saturation temperature is also shown. The reduction in saturation temperature at the interface causes a reduction in heat transfer through the liquid film compared to the case where noncondensables are absent.

1.2. Introduction to Condensing Heat Transfer

Figure 2a shows part of the sloping wall of the ice cavity and summarizes the various aspects of heat transfer involved. Heat is transferred from the cavity bulk vapor to the ice surface through two thermal resistances in series: a gas boundary layer and a liquid film of condensate and meltwater. The gas boundary layer resistance is principally due to the presence of noncondensable gases, which, in the context of this study, includes any gaseous component that does not condense or dissolve in the liquid film. The nature of this resistance is as follows. Flow from the bulk vapor to the liquid-vapor interface transports both steam, which condenses, and noncondensable gases, which accumulate at the interface (Figure 2b). At steady state, an equivalent diffusional counterflow of noncondensable gases away from the interface is driven by an elevated partial pressure of noncondensable gases at the interface. Since the total pressure remains constant, the partial pressure of steam at the interface is reduced. The condensing temperature of steam at the interface is thus reduced, which in turn reduces the temperature driving force for heat transfer across the liquid film [*Collier and Thome*, 1994].

The effect of noncondensable gases on condensing heat transfer is of considerable practical importance in engineering; particularly in the nuclear industry, where steam condensation in the presence of noncondensable gases is an important

mechanism for removing heat from a reactor containment vessel in the case of certain accident scenarios [*Anderson et al*., 1998; *De la Rosa et al*., 2009]. A reactor containment vessel is typically 20–30 m in diameter with the bulk flow in turbulent free convection during steam condensation once the initial reactor blowdown is complete [*Kim and Corradini*, 1990; *Kim et al*., 2009]. The extensive theoretical and experimental work devoted to quantifying steam condensation on the cooled surfaces of reactor containment vessels is thus of relevance to steam condensation on the roof and walls of a subglacial cavity.

2. Method

In this section we summarize the development of a model to estimate heat transfer rates during steam condensation. We review results for the condensation of pure vapors on vertical cooled surfaces, the extension to downward facing inclined cooled surfaces, and the modification required for simultaneous condensation and melting. We then consider condensation in the presence of noncondensable gases.

2.1. Condensation of a Pure Vapor on Vertical Cooled Surfaces

The analysis of condensation heat transfer can be traced back to Nusselt's 1916 paper [*Rose*, 1998], where he derived an equation for the heat transfer coefficient during condensation of a pure vapor on a vertical cooled surface. Nusselt's analysis was restricted to laminar flow in the condensate film. Subsequent work has considered condensation at higher film Reynolds numbers. The film Reynolds number, *Re*, is defined as

$$Re = 4G/\mu_l \tag{1}$$

where G is the mass flow rate of condensate per unit width of the film and μ_l is the condensate viscosity. The film surface is smooth for $Re < 30$. Above this value, ripples and waves form on the surface of the film: in this "wavy laminar" regime heat transfer increases, principally by reducing the average film thickness but also by increasing the area available for heat transfer. For $Re > 1600$, a fully turbulent, wavy film is developed [*Incropera and DeWitt*, 1996]. *Marto* [1998] presents a correlation of experimental results for the range $10 < Re < 31{,}000$:

$$Nu = 1.33Re^{-1/3} + 9.56 \times 10^{-6} Re^{0.89} Pr^{0.94} + 0.082 \tag{2}$$

where $Nu = U\,(\mu_l{}^2/\rho_l{}^2 g)^{1/3}/k_l$, U is the heat transfer coefficient, ρ_l and k_l are the liquid density and thermal conductivity respectively, g is the gravitational acceleration, and Pr is the liquid Prandtl number. The first term, which dominates at low *Re*, is similar to the classical form of the Nusselt equation [*Incropera and DeWitt*, 1996]:

$$Nu = 1.47Re^{-1/3} \tag{3}$$

2.2. Condensation of a Pure Vapor on Downward Facing Inclined Cooled Surfaces

Nusselt's original analysis was restricted to vertical surfaces. In a subsequent paper he considered condensation on the outside of a horizontal tube by proposing that, for a surface inclined at θ to the horizontal, the gravitational acceleration is "diluted" by a factor of $\sin\theta$ [*Rose*, 1998]. For inclined surfaces, this has proved to be an excellent modification, at least for large θ, even on downward facing surfaces, where the liquid film is subjected to a Rayleigh-Taylor type instability [*Gerstmann and Griffith*, 1967; *Piriz et al*., 2006].

Gerstmann and Griffith [1967] studied heat transfer for condensation on the underside of inclined surfaces, using Freon 113 as the condensing fluid and taking care to eliminate noncondensable gases. For inclinations greater than 15° from the horizontal their experimental results were within 10% of those predicted by the modified Nusselt equation. This result was corroborated by *Chung et al*. [2005], who condensed steam on downward facing plates as part of a wider study involving both steam and air.

2.3. Simultaneous Condensation and Melting of a Single Component

Most work on condensing heat transfer in the literature is concerned with condensation on cooled surfaces. For heat transfer within an ice cavity the latent heat of condensation melts the ice surface: the resultant liquid film thus comprises a mix of steam condensate and ice meltwater. Nusselt's analysis can be readily modified to allow for the thicker film that results. The heat transfer coefficient should be multiplied by a factor of $(1 + \lambda_v/\lambda_f)^{-1/4}$, where λ_v and λ_f are the latent heats of vaporization and fusion, respectively [*Eckhardt*, 1968]. For steam at 0.1 MPa this factor is 0.6 (0.64 at 4 MPa). The condensation of steam on ice in the presence of air was studied experimentally by *Yen et al*. [1973]. In their air-free experiments they found that simultaneous

condensation and melting effectively halved the heat transfer coefficient, compared with condensation on a surface cooled to 0°C.

2.4. Condensation in the Presence of Noncondensable Gases

Sections 2.1–2.3 developed a model for the heat transfer within the combined condensate and meltwater film on the ice surface. This section reviews models for the heat and mass transfer through the gas boundary layer that develops if noncondensable components are present in the bulk gas.

Analytical solutions of the boundary layer equations were achieved for simple geometries in the late 1960s [*Minkowycz and Sparrow*, 1966; *Sparrow et al*., 1967]. However, the solutions were too complex for practical application at the time; thus, industry relied on empirical correlations for the pragmatic solution of problems involving condensation in the presence of noncondensable gases [*Herranz et al*., 1998].

In the early 1990s, an alternative theoretical approach was developed that makes use of the analogy between heat and mass transfer in order to evaluate the mass transfer coefficients within the diffusional vapor-gas film. These heat and mass transfer analogy (HMTA) models or "diffusion layer models" [*Herranz et al*., 1998] became widely adopted within the nuclear and process industries [*De la Rosa et al*., 2009]. The development of the HMTA model is documented by *Collier and Thome* [1994]. We use the HMTA model, together with equation (2) with g replaced by $g \sin \theta$ for the liquid film resistance and the modification for simultaneous condensation and melting (section 2.3) to explore the effect of noncondensable gases' concentration and pressure on condensation in subglacial cavities.

The HMTA model requires evaluation of the heat transfer coefficient in the gas phase.

The intensity of free convection may be characterized by the Rayleigh number, Ra, defined as

$$Ra = \frac{g\alpha \Delta \mathrm{T} \mathrm{d}^3}{\kappa \nu} \tag{4}$$

where g is the gravitational acceleration, ΔT is the temperature difference, d is the vertical dimension of the convective motion, and α, κ, and ν are the coefficients of thermal expansion, thermal diffusivity, and kinematic viscosity, respectively, of the fluid [*Turner*, 1973]. For Rayleigh numbers appropriate to convection in subglacial cavities, the heat transfer coefficient over a smooth surface inclined at an angle θ to the horizontal may be obtained from the Nusselt number, Nu, given by [*Raithby and Hollands*, 1998]

$$Nu = \max\left\{0.13\,(Ra\,\sin\,\theta)^{1/3},\ 0.14\,(Ra\,\cos\,\theta)^{1/3}\right\} \tag{5}$$

where Nu is defined as Ud/k_f, with free convection heat transfer coefficient U and fluid thermal conductivity k_f.

The resulting heat transfer coefficient needs to be enhanced by a factor to allow for the roughness of the liquid film surface. *Kim et al*. [2009] carried out a wide-ranging study of condensation in the presence of noncondensable gases for pressures in the range 0.4–2.0 MPa. We have used their data, together with the HMTA model, to determine an appropriate enhancement factor (*EF*). This appears to be independent of the mole fraction of noncondensable gases but depends on pressure. The resulting equation for the enhancement factor is

$$\mathrm{EF} = 2.6 + 0.4P \tag{6}$$

where P is the pressure in MPa.

The study by *Kim et al*. [2009] was restricted to vertical surfaces. *Huhtiniemi and Corradini* [1993] studied condensation heat transfer in the presence of noncondensable gases at atmospheric pressure for a range of downward facing surface orientations. They found little effect of orientation on heat transfer coefficient, suggesting that the enhancement factor might be independent of orientation. Furthermore, their data can be reproduced well by our HMTA model with an enhancement factor of 2.6 (appropriate to 0.1 MPa).

3. Results

3.1. General Results for the HMTA Model

Figure 3 shows overall heat transfer coefficients versus mole fraction of noncondensable gases in the bulk vapor, for various total cavity pressures and liquid film lengths. In all cases the overall heat transfer coefficient decreases with an increase in the mole fraction of noncondensable gases. Similar trends in overall heat transfer

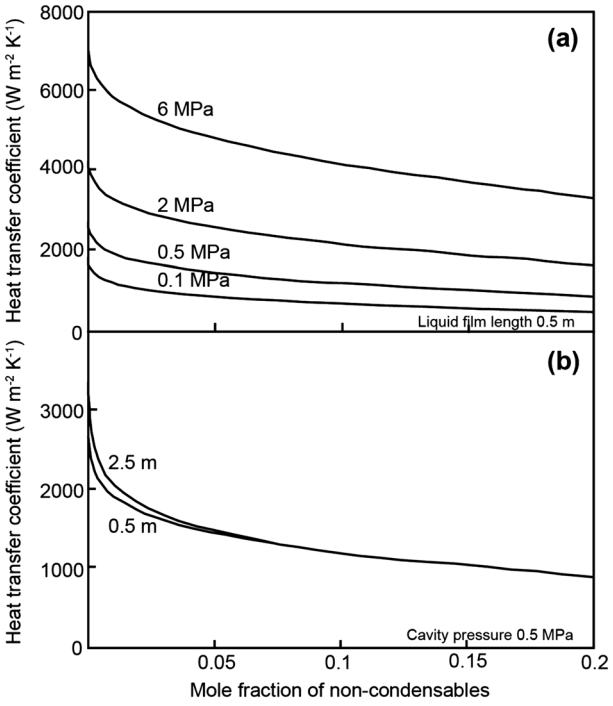

Figure 3. Heat transfer coefficients from bulk cavity fluid to the ice wall (inclined at 15°) versus mole fraction of noncondensable gases in the bulk vapor. (a) The effect of cavity pressure, for a liquid film length of 0.5 m. (b) The effect of liquid film length at a cavity pressure of 0.5 MPa.

coefficient with noncondensable gas mole fraction have been reported in the literature. *Chung et al.* [2005] performed a series of steam condensation experiments at atmospheric pressure on a water-cooled flat plate, while varying the plate inclination and the proportion of air in steam. Their results showed a systematic reduction of overall heat transfer coefficient with increasing proportion of air. Heat transfer coefficients are relatively insensitive to liquid film length except at very low ($<$0.01) mole fraction of noncondensables.

3.2. Application to Subglacial Cavities

The general behavior of the HMTA model suggests that heat transfer coefficients depend mainly on bulk noncondensables' mole fraction and cavity pressure. This section attempts to estimate the likely range of heat transfer coefficients that might be obtained in drained subglacial cavities.

3.2.1. The Effect of Noncondensable Gases

Höskuldsson and Sparks [1997] suggested that noncondensable gases could be sourced from air released from ice on melting and from insoluble components of volcanic gases. Air in glacial ice originates as air trapped within firn [*Martinerie et al.*, 1992]. Firn is permeable to air, so during compaction any excess air can be vented to the surface via a network of interconnecting channels. At a "critical" depth of around 50–100 m this connection to the surface becomes broken and air, at atmospheric pressure, becomes trapped as air bubbles. The amount of air released on melting can be estimated, given that firn voidage at the critical depth is around 0.1 [*Martinerie et al.*, 1992]. Thus, at the critical depth, 1 m^3 of firn comprises 0.9 m^3 of pure ice (around 828 kg) and 0.1 m^3 of air at atmospheric pressure (around 0.13 kg). Hence, around 0.16 kg of air per ton (10^3 kg) of ice will be released on melting.

Sigvaldson and Elisson [1968] present chemical analyses of volcanic gas from the 1965 Surtsey eruption. A typical analysis, for a case where there is minimal contamination by ambient air, is presented in Table 1. Both HCl and SO_2 are highly soluble in water and can be expected to dissolve completely in meltwater, while H_2 and CO are substantially insoluble in water. CO_2 is partly soluble in water, dependent on its partial pressure and water temperature.

To establish the likely concentrations of noncondensable gases, we assume for illustrative purposes a subglacial eruption of basaltic magma in a drained cavity filled with saturated steam at 1.5 MPa. If the magma cools from an eruption temperature of around 1200°C to a glass at 200°C, the heat released is 1200 kJ per kg magma, assuming an average glass specific heat capacity of 1.2 kJ kg^{-1} K^{-1} [*Höskuldsson and Sparks*, 1997]. If the heat

Table 1. Volcanic Gas Composition From 1965 Surtsey Eruption

	Component						
	H_2O	HCl	SO_2	CO_2	H_2	CO	Total
Mole[a] %	86.1	0.4	2.7	5.7	4.7	0.4	100.0
Weight %	77.1	0.7	8.6	12.5	0.5	0.6	100.0

[a]Table 1 (average for 21 February) in *Sigvaldson and Elisson* [1968].

released melts ice and heats meltwater to 20°C, the amount of ice melted is thus 1200/(335 + 4.2 × 20) or around 3 kg per kg magma, where the latent heat of fusion of ice is 335 kJ kg^{-1} and the specific heat capacity of water is 4.2 kJ kg^{-1} K^{-1} [*Rogers and Mayhew*, 1980]. For each ton of magma, the size of the cavity produced is thus around 3.3 m^3 and the amount of air released by melting the ice is around 0.5 kg.

Mid-ocean ridge basalt and ocean island basalt magmas contain less than 1% weight of volatiles on eruption [*Wallace and Anderson*, 2000]. One ton of magma containing 1% of gas with the composition presented in Table 1 would release 0.11 kg of H_2 and CO together with 1.25 kg of CO_2 as potential noncondensable gases. CO_2 solubility is limited at 200°C (the temperature of the steam-water interface in the cavity), given the relatively low partial pressure of CO_2 in the cavity. The total amount of noncondensable gases is thus around 1.5–2 kg per ton of magma. If the cavity produced by the eruption is drained, it will be filled with saturated steam at 200°C with a density of 8.1 kg m^{-3} [*Rogers and Mayhew*, 1980]. A cavity of 3.3 m^3 thus contains 27 kg steam. The corresponding level of noncondensable gases in the steam is thus around 5 weight %; corresponding to a mole fraction of 0.02.

The calculation above assumes that the cavity produced is empty; in practice some of the cavity (around 10–20%) will be occupied by the volcanic edifice. Furthermore, if the cavity is significantly underpressured (compared with glaciostatic conditions) then the cavity will progressively collapse by ductile ice flow [*Tuffen*, 2007]. Both effects will reduce the space available for the noncondensable gases and thus increase their concentration within the cavity. The Katla 1918 eruption penetrated the overlying ice in 2 h [*Gudmundsson*, 2005], and there was probably little ductile movement in the overlying ice during the subglacial stage of the eruption. For the Gjálp 1996 eruption, the overlying ice was penetrated in 30 h [*Gudmundsson et al*., 2004], allowing sufficient time for ductile ice flow to reduce cavity size (depressions were observed in the ice surface above the eruption site). It seems likely that, in the case of the Gjálp 1996 eruption, the concentration of noncondensable gases in the cavity may have been considerably greater than 5 weight % unless they were removed from the cavity.

A possible way of removing noncondensable gases from the cavity might be by venting them to the surface up a crevasse in the ice. *Gudmundsson et al*. [2004] noticed the presence of en echelon fractures on the ice surface above the Gjálp 1996 site before the eruption became subaerial. They suggested that the fractures may be the surface expression of a basal crevasse that was produced by tensional stresses associated with dyke intrusion at the start of the subglacial eruption and that fractures might be of the order of 1 m wide.

If a fracture in the ice exists from cavity to surface, then a mixture of steam and noncondensable gases may vent from the cavity. During flow up in the fracture, steam would progressively condense and melt back the walls of the fracture, thus mitigating the tendency for ductile ice flow to close the fracture (note that both creep rates and meltback rates increase downward). If the fracture is sufficiently wide, the combined liquid flow of condensate and meltwater will reflux back down the fracture. Application of the "flooding equation" [*Kay and Nedderman*, 1985] suggests that liquid can reflux if the fracture is wider than 0.5 m. Note that the flooding equation is applicable to vertical circular pipes and may not be appropriate for a channel with parallel walls. At the surface, only the noncondensable gases would be vented; these would not be visible from the air; however, it might be possible to detect elevated levels of noncondensable gases above the fractures.

3.2.2. Implications for Heat Fluxes in Drained Subglacial Cavities

In section 4.1 we suggest that liquid film thickness is unlikely to increase for film lengths above 0.5 m. The discussion in section 3.2.1 suggests that the mole fraction of noncondensables is likely to be at least 0.02 but that it is difficult to set an upper limit. For a liquid film length of 0.5 m and a mole fraction of noncondensables of 0.02, Figure 3 indicates that heat transfer coefficients range from 1 to 4 kW m^{-2} K^{-1} over the pressure range 0.1 to 4 MPa. The corresponding heat fluxes are thus 0.1 to 1 MW m^{-2}.

A condensing heat flux of 1 MW m^{-2} will melt ice with a vertical penetration rate of around 12 m h^{-1} if meltwater leaves the ice cavity surface at 0°C. If the meltwater temperature is 100°C the corresponding rate is 5 m h^{-1}. Ice penetration rates of 16 and 50 m h^{-1} were inferred for the Gjálp 1996 eruption [*Gudmundsson et al*., 2004] and the 2010 Eyjafjallajökull eruption [*Magnússon et al*., 2012], respectively. Thus, heat fluxes from steam condensation appear to be considerably smaller than those inferred from recent subglacial eruptions. We speculate that, if a steam layer undergoing free convection developed during the Gjálp 1996 subglacial eruption, it was only present for part of the eruption and that other, more efficient, ice penetration mechanisms were present at other times. We consider possible ways of enhancing the steam condensation in section 3.2.3.

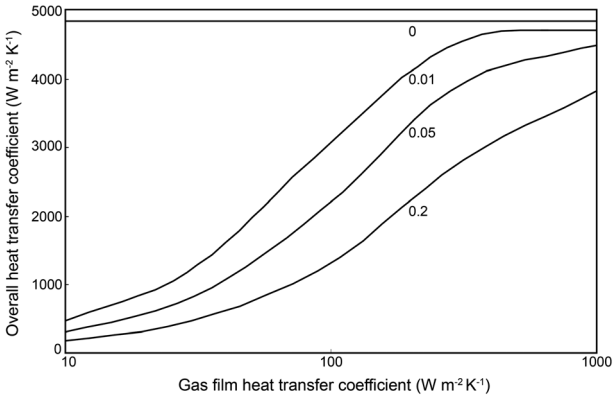

Figure 4. Variation of overall heat transfer coefficient with gas film heat transfer coefficient for a range of noncondensable mole fractions. Condensation and melting at 2 MPa with a liquid film length of 0.5 m on an ice cavity wall inclined at 15°.

3.2.3. Forced Convection in Steam-Dominated Cavities

The results presented in section 3.2.2 assume that heat transfer in the gas phase is by free convection; in some instances, convection within the gas phase may be enhanced by momentum transfer from an eruption jet.

Figure 4 shows the variation of overall heat transfer coefficient (OHTC) with gas film heat transfer coefficient h_f. Figure 4 was developed from a modified version of the HMTA model where h_f can be varied independently rather than calculated from equation (5). At 2 MPa, values of h_f of 100 W m^{-2} K^{-1} are typical of free convection. As h_f increases the heat transfer resistance of the gas-vapor film decreases, and the OHTC is increasingly determined by the heat transfer of the liquid film. In this case a factor of 2–3 increase in the OHTC can be obtained, depending on the concentration of noncondensables present. Forced convection within a steam-dominated cavity may thus melt ice with an ice penetration rate to match that inferred for the Gjálp 1996 eruption.

It is possible that the overall heat transfer coefficient could be increased further by impingement of the magmatic eruption jet onto the ice surface, causing local thinning of the liquid film. However, this would require the jet to be optimally placed relative to the ice surface, which is unlikely. Furthermore, any enhancement in melting rate would be restricted to the immediate locality around the impingement zone; the rest of the cavity roof would remain largely unaffected.

3.3. Thermal Dynamics of Steam-Dominated Cavities

The model presented in sections 2 and 3 so far assumes steady state heat transfer, where steam condensation rates are balanced by steam generation rates and cavity pressure is constant. In this section we consider the thermal dynamics of a steam-dominated cavity in response to changes in steam generation rate. Such changes may be caused by changes in magma input or by changes in the efficiency of heat transfer from magma to water, for example, by changes in the degree of magma fragmentation. One might expect that a steam-dominated cavity would have a small thermal capacity and thus a dynamic response that is orders of magnitude faster than the equivalent liquid-filled cavity. Such rapid changes in cavity conditions may have implications for ice-melting rates and thus for the development of the associated eruption hazards. In this section we show that, if vapor-liquid equilibrium is maintained, the effective thermal capacity is dominated by latent heat changes that are much larger than sensible heat changes.

Consider a cavity at steady state that is subjected to a sudden increase in steam generation rate. Cavity pressure will increase, along with cavity temperature if thermal equilibrium between steam and liquid water is maintained. The temperature of the magma provides the ultimate upper bound on cavity temperature; however, we restrict our discussion to cavity temperatures below the critical temperature of water. Under this restriction, cavity pressure may increase up to the critical pressure of 22.1 MPa. The glaciostatic head of ice equivalent to the critical pressure is around 2500 m; thus, the ice sheet surrounding a subglacial eruption might be expected to lift or to fracture in most if not all terrestrial subglacial eruptions.

For illustrative purposes, we estimate the time taken for cavity pressure to double in response to a doubling of steam generation rate. For expediency, we consider a triangular cavity of height H and base $2\beta H$ that develops over a linear eruption fissure. The surface area for steam condensation per unit length of fissure is thus $2H\,(1+\beta^2)^{1/2}$. For a condensation heat transfer coefficient U and a steady state cavity temperature T_{so}, the condensing heat load Q (equal to the steam generation heat load in steady state) is given by

$$Q = 2UT_{so}H\left(1+\beta^2\right)^{1/2} \tag{7}$$

Table 2. Evaluation of the Finite Difference $\Delta T_s / \Delta \rho_g$ (Equation (14)) Evaluated Over a Range of Cavity Pressures[a]

	Cavity Pressure (MPa)							
Variable	1.0	2.0	3.0	4.0	5.0	6.0	7.0	8.0
T_s (°C)	179.9	212.4	233.8	250.3	263.9	275.6	285.8	295.0
h_g (kJ kg^{-1})	2778	2799	2802	2801	2794	2784	2772	2758
ρ_g (kg m^{-3})	5.144	10.04	15.00	20.09	25.35	30.83	36.54	42.52
ΔT_s (°C)		32.5	21.4	16.5	13.6	11.7	10.2	9.2
$\Delta \rho_g$ (kg m^{-3})		4.90	4.96	5.09	5.26	5.48	5.71	5.98
$\Delta T_s / \Delta \rho_g$ (°C m^3 kg^{-1})		6.6	4.3	3.2	2.6	2.1	1.8	1.5

[a]Values for saturation temperature (T_s), saturated steam enthalpy (h_g) and density (ρ_g) from *Rogers and Mayhew* [1980].

The steam generation heat load is then stepped up to 2Q. If the condensation heat transfer coefficient U remains constant, the condensation heat load increases to QT_s/T_{so} for a cavity temperature T_s that increases with time. The heat accumulation rate in the cavity, A_C, is thus given by

$$A_C = Q(2 - T_s/T_{so}) \tag{8}$$

which is equal to the rate of change of cavity heat content with time.

The cavity heat content H_c, relative to liquid water at 0°C, is given by

$$H_c = m_l h_l + m_g h_g \tag{9}$$

where m_l and m_g are the masses of liquid water (with enthalpy h_l) and steam (with enthalpy h_g) in the cavity. We consider the case where m_l may be neglected but there is sufficient liquid water present to maintain vapor-liquid equilibrium as cavity pressure increases and liquid water is turned to steam. An upper limit on the rate of change of cavity heat content with time is thus given by

$$\frac{dH_c}{dt} = \frac{d(m_g h_g)}{dT_s} \times \frac{dT_s}{dt} \tag{10}$$

which may be expanded to

$$\frac{dH_c}{dt} = \frac{dT_s}{dt} \times \left(m_g \frac{dh_g}{dT_s} + h_g \frac{dm_g}{dT_s} \right). \tag{11}$$

The enthalpy of steam, h_g, is almost independent of temperature over the range of interest (see Table 2); thus, equation (11) becomes

$$\frac{dH_c}{dt} = h_g \frac{dT_s}{dt} \times \frac{dm_g}{dT_s}. \tag{12}$$

For a cavity volume of βH^2 per unit length of eruption fissure, the mass of steam in cavity is $\rho_g \beta H^2$, where ρ_g is the density of steam. Equation (12) thus becomes

$$\frac{dH_c}{dt} = h_g \frac{dT_s}{dt} \times \beta H^2 \frac{d\rho_g}{dT_s}. \tag{13}$$

The effective thermal capacity per unit volume for a vapor-dominated cavity in which vapor equilibrium is maintained is given by $h_g \, d\rho_g/dT_s$. This is a latent heat term that is much larger than the sensible heat term $\rho_g C_{pg}$ in the case where vapor equilibrium is not maintained.

Combination of equations (7), (8), and (13) yields, after rearrangement

$$\frac{dT_s}{dt} = \frac{UT_{so}(2 - T_s/T_{so})}{h_g} \times \frac{2\left(1 + \beta^2\right)^{1/2}}{\beta H} \times \frac{dT_s}{d\rho_g}. \tag{14}$$

The rate of increase of cavity temperature with time may be determined approximately by replacing differential terms by finite differences. The finite difference $\Delta T_s/\Delta \rho_g$ is evaluated over a range of cavity temperatures in Table 2.

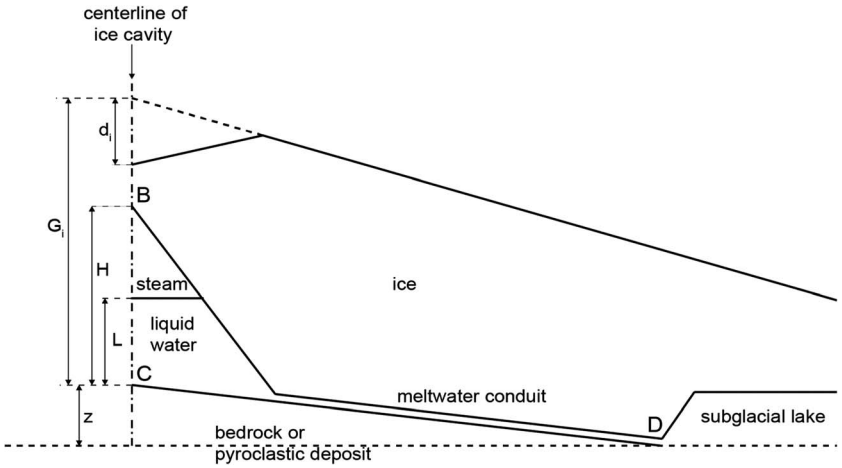

Figure 5. Schematic diagram of one half of a subglacial eruption cavity that drains meltwater into a subglacial lake, showing symbols used in section 3.4. Volcanic edifice not shown.

For illustration, consider a cavity with a height H of 50 m, with $\beta = 2$, and a condensing heat transfer coefficient U of 2300 W m^{-2} K^{-1}. For a cavity pressure increase from 2 to 4 MPa, temperature increases at around 0.03 K s^{-1}; the pressure increase thus takes around 20 min. This estimate could be refined by considering alternative cavity shapes, the increase in condensing heat transfer coefficient with pressure, or variation in steam volume (perhaps produced by changes in water level in the cavity). The corresponding time for a liquid-dominated cavity of the same size to respond to the same change in heat input is around 2 h, around 6 times slower.

3.4. Conditions for the Existence of a Partly Flooded Subglacial Eruption Cavity

Figure 1 shows a case where a subglacial eruption cavity is partly drained. Here meltwater discharges from the cavity via a meltwater pathway in the ice into a subglacial lake. Under some conditions, a steam-liquid water interface can be present in the cavity, with the equilibrium level L of the interface determined by

$$P_{\text{steam}} + L\rho_l g = P_{\text{D}} + \Delta P_f \tag{15}$$

where P_{steam} is the steam pressure in the cavity, ρ_l is the density of liquid water, g is the gravitational acceleration, P_{D} is the static pressure at the point where the meltwater enters the subglacial lake and ΔP_f is the frictional pressure loss in the conduit. Variation of the interface level in the cavity has the potential to vary meltwater flow rates and to vary the meltwater production rates if heat transfer rates above and below the interface are significantly different.

We examine in more detail the conditions under which a steam-liquid water interface may exist within a subglacial cavity. Figure 5 shows a cross section along the meltwater drainage route from the center line of a cavity of height H to a subglacial lake where the meltwater accumulates. The extent of drainage of the cavity may be quantified by L/H, with the depth of liquid water L in the cavity determined by considering the static pressure balance within the system.

At the top of the cavity (point B in Figure 5), the pressure P_{B} is determined by the thickness of ice and any shear stress within the ice that reduces the glaciostatic pressure (this shear stress develops as a consequence of progressive ductile collapse of the cavity roof as the cavity grows) [*Gudmundsson et al.*, 2004]:

$$P_{\text{B}} = (G_i - d_i - H)\rho_i g - \tau \tag{16}$$

where G_i is the preeruption thickness (for the current eruption) of ice above bedrock, d_i is the depth of any depression that develops in the ice surface and τ is the underpressure: the reduction in glaciostatic pressure due to shear stress in the ice. The pressure at point C at the base of the cavity is thus

$$P_{\text{C}} = P_{\text{B}} + L\rho_l g \tag{17}$$

if the density of steam is neglected. The pressure at point D at the entrance to the subglacial lake is thus

$$P_{\text{D}} = P_{\text{C}} + z\rho_l g - \Delta P_f \tag{18}$$

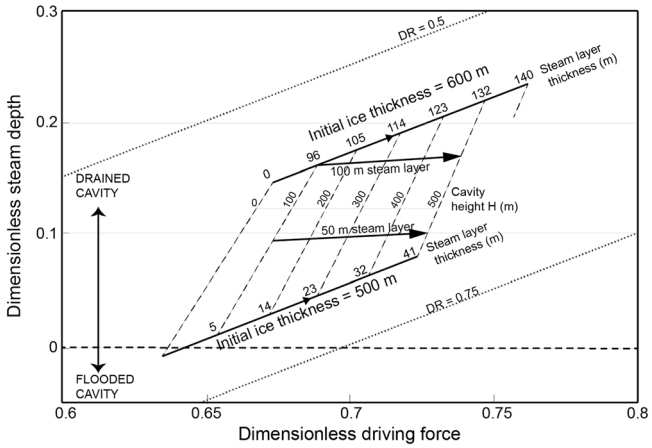

Figure 6. Dimensionless steam depth versus dimensionless driving force for meltwater drainage during subglacial eruption cavity development. Dotted lines are lines of constant dimensionless resistance (DR) to meltwater flow. The diagonal solid lines represent the development of two specific eruption cases (with constant DR), using Gjálp 1996 eruption data but for different initial ice thicknesses. Dashed lines join points of constant cavity height. Two additional solid lines identify the 50 m and 100 m constant steam depth cases discussed in section 3.4.

where ΔP_f is the frictional pressure drop due to flow of meltwater from C to D and z is the elevation of C above D. Elimination of P_B and P_C from equations (16) to (18) and rearrangement yields

$$L = \frac{(P_D + \tau + \Delta P_f)}{\rho_l g} - \frac{(G_i - d_i - H)\rho_i}{\rho_l} - z \qquad (19)$$

We consider equation (19) in the context of the Gjálp 1996 subglacial eruption. Figure 14a in *Gudmundsson et al.* [2004] shows a cross section, part way through the subglacial eruption, along the meltwater path from the eruption site to Grimsvötn. This shows a thickness, h, of 370 m of ice where meltwater enters Grimsvötn. In general, the glaciostatic pressure is given by $h\rho_i g$, where ρ_i is the density of ice (911 kg m^{-3}) and g is the gravitational acceleration (9.81 m s^{-2}). The pressure P_D, for this specific case, is thus 3.3 MPa. The elevation difference between points C and D in Figure 5 for this case is approximately 40 m. Equation (19) can be used to estimate the ice thickness required for a steam layer, of thickness $(H - L)$, to exist at the top of a partly flooded subglacial cavity. *Gudmundsson et al.* [2004] suggested that the underpressure in the ice τ lies in the range 1–2 MPa. The frictional pressure drop is likely to be small compared to τ: we estimate a value for ΔP_f of 0.1 MPa in Appendix A.

For illustrative purposes we consider the case with τ equal to 1.5 MPa. As cavity height H increases from 100 m to 500 m, the ice thickness G_i required for a 50 m thick steam layer decreases from 549 m to 510 m. For a 100 m thick steam layer the corresponding ice thickness required decreases from 604 m to 565 m. An increase in τ of 0.5 MPa increases the required ice thickness by 56 m. Figure 14a in *Gudmundsson et al.* [2004] shows a preeruption ice thickness of around 600 m. It is thus plausible that the Gjálp 1996 subglacial eruption cavity was partly steam filled. In practice, large cavity heights may be infeasible if surface fractures in the ice extend through the cavity roof.

Equation (19) may be generalized by defining a "dimensionless steam depth":

$$\frac{H - L}{G_i} = \frac{(G_i - d_i - H)\rho_i/\rho_l - \tau/\rho_l g + H + z}{G_i} - \frac{P_D + \Delta P_f}{\rho_i g G_i} \qquad (20)$$

The second term on the right-hand side (RHS) is a "dimensionless resistance" to the flow of meltwater, comprising both backpressure (P_D) and frictional drop ΔP_f. The first term on the RHS may be considered as a dimensionless driving force. A subglacial cavity is just flooded (full of liquid water) when $L = H$, i.e., when the dimensionless steam depth is zero. A subglacial cavity is just drained when $L = 0$, i.e., when the dimensionless steam depth is H/G_i. Negative values of dimensionless steam depth indicate that there is insufficient glaciostatic head above the top of the cavity to allow meltwater to drain, even when full of liquid water. In practice, negative values of dimensionless steam depth are infeasible: in this case τ would decrease to the point that meltwater could drain from the liquid-filled cavity.

Figure 6 shows a graph of dimensionless steam depth versus dimensionless driving force for two values of dimensionless resistance. Data specific to a developing subglacial eruption may be plotted onto Figure 6. For illustration, two cases are plotted, using the Gjálp eruption data and a constant value of τ but with different initial ice thicknesses. We assume here that d_i and ΔP_f are constant, although they are expected to increase and decrease respectively as the cavity develops. For an initial ice thickness of 500 m the cavity is initially flooded (dimensionless steam depth < 0) but develops a steam layer as cavity height increases. For an

initial ice thickness of 600 m the cavity is fully drained until the cavity height is around 100 m and then partly drained for the remainder of its development, with the steam layer increasing in thickness to 140 m. Development of a steam layer in a cavity is thus favored by thick ice that provides sufficient glaciostatic pressure to balance the resistance to meltwater drainage.

4. Discussion

In this section we discuss controls on liquid film length and thickness during steam condensation, compare steam condensation heat fluxes with likely heat fluxes from other heat transfer mechanisms, and consider the effect of tephra in the system.

4.1. Controls on Liquid Film Length and Thickness

On a vertical surface, the liquid film length can extend down the full height of the surface. Irregularities in the sloping surface of the ice cavity may limit the length of a liquid film, with shedding of the film if a local discontinuity of slope is sufficiently abrupt. We anticipate that the cavity surface may be fractured by magmatic and phreatomagmatic explosive activity; in this case liquid film length will depend on the degree to which the cavity surface is fractured. Fracturing will also increase the ice surface area available for heat transfer. We are not aware of information in the literature on fracture spacing due to explosions under ice.

There is some evidence that the film thickness may be self-limiting. On downward facing inclined surfaces, *Gerstmann and Griffith* [1967] observed that the condensate film developed into a series of longitudinal ridges and troughs and that condensate rained from the ridges. They envisaged a steady state in which much of the condensation took place at the thin film in the troughs and that condensate flow had a lateral component into the ridges, where it was removed from the surface by droplet shedding. Under this scenario, a condensate film may attain a constant average thickness, rather than increasing along its length.

Gerstmann and Griffith [1967] observed that the location of the transition between the initially smooth film and the alternating ridges and troughs moved up the downward facing inclined surface as heat flux, and thus condensation rate, increased. In all cases they observed that the transition occurred within the length of the surface in their apparatus (approximately 0.5 m). For the case of simultaneous condensation and melting, in which the liquid flux in the film is increased by an order of magnitude compared with the simple cooled surface case, one might expect an earlier transition to ridges and troughs.

Gerstmann and Griffith's work was carried out with Freon 113, rather than water. *Anderson et al*. [1998] observed similar behavior for the condensation of steam on the underside of a cooled curved surface that increased in inclination from horizontal to 15° over a 1.8 m length. We tentatively conclude that, for simultaneous condensation and melting on a downward facing inclined surface, a maximum average film thickness might be attained after 0.5 m.

4.2. Comparison of Steam Condensation With Other Heat Transfer Mechanisms

In section 3.2.2 we show that, in vapor-dominated cavities, heat fluxes of 0.1–1 MW m^{-2} can be obtained by steam condensation where the bulk steam undergoes free convection and we anticipate heat fluxes up to 2 MW m^{-2} for forced convection. For liquid-dominated cavities, 0.1 to 1 MW m^{-2} may be achieved by single-phase free convection, with heat fluxes of 3–5 MW m^{-2} estimated for two-phase free convection [*Woodcock et al*., 2014]. Thus, steam condensation heat fluxes are similar to those likely to be achieved by single-phase convection in liquid-filled cavities but smaller than heat fluxes estimated for two-phase free convection. In a partly liquid-filled cavity undergoing two-phase free convection, sideways melting rates may be considerably greater than upward melting rates. This is similar to the findings of *Höskuldsson and Sparks* [1997], who produced pancake-shaped cavities when an insulating layer of air developed at the top of cavities in their experiments to melt ice by single-phase convection of liquid water.

An alternative ice-melting mechanism, in which heat is transferred directly from magma to ice, was proposed by *Wilson and Head* [2002] for basaltic magmas. They proposed that a depressurized (i.e., atmospheric pressure) subglacial cavity may be produced if a connection to the atmosphere can be established. Depressurization of the cavity initiates a Hawaiian-style lava fountain that "drills" through the overlying ice by pyroclast impact up to the unconstrained height of the fountain. Melting of the cavity then continues by

radiative heat transfer from the lava fountain [*Wilson and Head*, 2002]. The heat fluxes in this scenario remain to be quantified.

4.3. The Effect of Tephra in the System

A vapor-dominated cavity will contain a "dusty gas" comprising tephra as well as steam. The model of steam condensation heat transfer presented in this paper considers the tephra-free end-member and thus assesses the contribution of steam condensation to ice-melting rates.

Replacing pure steam by a dusty gas with a higher density and specific heat capacity increases the rate of transport of heat within the cavity, provided that convection velocities are not decreased by the higher density. Tephra particles may be carried up to the cavity roof with sufficient momentum to mechanically abrade the ice surface. In addition, the presence of particles enhances heat transfer coefficients within the liquid film on the ice surface [*Ozbelge*, 2001]. The presence of tephra may thus increase heat fluxes; however, the effect of tephra in the system remains to be quantified.

5. Conclusions

We have used published heat transfer calculation methods to estimate steam condensation heat fluxes on the ice-melting surfaces within vapor-dominated subglacial cavities during explosive volcanic eruptions. The principal conclusions are as follows.

1. Heat fluxes of 0.1–1 MW m^{-2} can be obtained by steam condensation in vapor-dominated cavities where the bulk steam undergoes free convection. These heat fluxes are similar to estimates of heat flux from single-phase convection in liquid-filled cavities.
2. Forced convection of the bulk steam reduces the thermal resistance of the gas boundary layer and thus increases the condensing heat flux to the point where heat transfer is determined by the resistance of the liquid film. In this case a maximum heat flux of 2 MW m^{-2} may be obtained; this may produce ice penetration rates that match those inferred from recent subglacial eruptions.
3. Vapor-dominated cavities in which vapor-liquid equilibrium is maintained have thermal dynamic responses that are an order of magnitude faster than the equivalent flooded cavities.

Appendix A: Frictional Pressure Drop in Subglacial Conduits

The frictional pressure drop ΔP_f due to the flow of a fluid in a conduit of circular cross section with length L_e and diameter D is given by:

$$\Delta P_f = C_f \times \left(\frac{L_e}{D}\right) \times 0.5 \rho v^2 \tag{A1}$$

where ρ and v are the density and velocity of the fluid, respectively. C_f is the friction coefficient which depends on the Reynolds number of the flow and the relative roughness of the conduit wall [*Massey*, 1970]. The flow rate of fluid q is as follows:

$$q = \pi D^2 v / 4 \tag{A2}$$

For the Gjálp 1996 eruption considered in section 3.4 the flow rate was 0.5 km^3 per day for the first two days of the eruption [*Gudmundsson et al*., 2004] or 6000 $m^3\,s^{-1}$.

We expect the water velocity in the conduit to be in the range 1–10 m s^{-1}; thus, the diameter of a single conduit will be in the range 30–90 m. The corresponding flow Reynolds number is thus 10^7–10^8; under these fully turbulent flow conditions the friction coefficient is around 0.005 [*Massey*, 1970]. The frictional pressure drop may then be evaluated from equation (A1); it lies in the range 250 to 10^5 Pa.

A conduit of 30 m diameter is unlikely to be present at the start of the eruption, but may develop from an existing subglacial drainage channel by the passage of warm meltwater. We estimate the rate at such a conduit might develop by noting that 0.21 km^3 of ice melted in 3 days along the conduit from the Gjálp 1996 subglacial eruption site to the subglacial lake Grimsvötn, a distance of around 10 km [*Gudmundsson et al*., 2004]. The variation of melting rate with time during the 3 day period is not known; for the purpose of

illustration we assume that it is constant at the average value of 810 $m^3 s^{-1}$. The rate of change of conduit radius R with time is thus given by

$$\frac{dR}{dt} = \frac{810}{2\pi R L_e} \tag{A3}$$

where L_e is the conduit length. Integration of equation (A3) between the limits on R of 0 to 15 m yields a time of 2.5 h.

Notation

A_C heat accumulation rate in the cavity, W.
C_f friction factor, dimensionless.
C_{pg} vapor specific heat capacity, J $kg^{-1} K^{-1}$.
D diameter of conduit of circular cross section, m.
d vertical dimension for convection, m.
d_i depth of depression in ice surface, m.
EF enhancement factor for heat transfer coefficient, dimensionless.
G mass flow rate per unit width, kg $s^{-1} m^{-1}$.
G_i thickness of ice above bedrock, m.
g acceleration due to gravity, m s^{-2}.
h ice thickness, m.
H cavity height, m.
H_c cavity heat content, J.
h_f gas-vapor film heat transfer coefficient, W $m^{-2} K^{-1}$.
h_g saturated vapor specific enthalpy, kJ kg^{-1}.
h_l saturated liquid specific enthalpy, kJ kg^{-1}.
k_f fluid thermal conductivity, W $m^{-1} K^{-1}$.
k_l liquid thermal conductivity, W $m^{-1} K^{-1}$.
L depth of liquid water in subglacial cavity, m.
L_e length of conduit, m.
m_g mass of steam in cavity, kg.
m_l mass of liquid water in cavity, kg.
Nu Nusselt number, dimensionless.
P pressure, Pa.
P_B pressure at top of subglacial cavity, Pa.
P_C pressure at bottom of subglacial cavity, Pa.
P_D static pressure where the meltwater enters subglacial lake, Pa.
P_{steam} steam pressure in the subglacial cavity, Pa.
Pr Prandtl number, dimensionless.
q fluid flow rate, $m^3 s^{-1}$.
Q heat rate, J s^{-1}.
R conduit radius, m.
Ra Rayleigh number, dimensionless.
Re Reynolds number, dimensionless.
T_s cavity temperature, K.
T_{so} steady state cavity temperature, K.
t time, s.
U heat transfer coefficient, W $m^{-2} K^{-1}$.
v fluid velocity, m s^{-1}.
z height of base of subglacial cavity above bottom of subglacial lake, m.
α coefficient of thermal expansion, K^{-1}.
β ratio of cavity half width to height, dimensionless.
ΔP_f frictional pressure loss, Pa.

ΔT temperature difference, K.
κ thermal diffusivity, $m^2\,s^{-1}$.
λ_f fluid latent heat of fusion, $J\,kg^{-1}$,
λ_v fluid latent heat of vaporization, $J\,kg^{-1}$.
μ_l liquid dynamic viscosity, Pa s.
ν kinematic viscosity, $m^2\,s^{-1}$.
ρ fluid density, $kg\,m^{-3}$.
ρ_g vapor density, $kg\,m^{-3}$.
ρ_i ice density, $kg\,m^{-3}$.
ρ_l liquid density, $kg\,m^{-3}$.
τ underpressure, Pa.
θ angle of inclination of surface to horizontal, degree.

Acknowledgments
The data supporting this paper are available as supporting information. We thank two anonymous reviewers for their detailed comments during review which have enabled us to improve the paper. We are grateful to Lionel Wilson for comments on an early version of this paper.

References

Anderson, M. H., L. E. Herranz, and M. L. Corradini (1998), Experimental analysis of heat transfer within the AP600 containment under postulated accident conditions, *Nucl. Eng. Des.*, *185*, 153–172.
Chung, B.-J., S. Kim, and M. C. Kim (2005), Film condensations of flowing mixtures of steam and air on an inclined flat plate, *Int. Comm. Heat Mass Tran.*, *32*, 233–239.
Collier, J. G., and J. R. Thome (1994), *Convective Boiling and Condensation*, Clarendon Press, Oxford, U. K.
De la Rosa, J. C., A. Escriva, L. E. Herranz, T. Cicero, and J. L. Munoz-Cobo (2009), Review on condensation on the containment structures, *Prog. Nucl. Energy*, *51*, 32–66.
Eckhardt, H. H. (1968), Die Wärmeübertragung von kondensierendem Dampf an schmelzende Wände (The transfer of heat from condensing steam to melt walls), *Chem. Ing. Tech.*, *40*, 488–494.
Gerstmann, J., and P. Griffith (1967), Laminar film condensation on the underside of horizontal and inclined surfaces, *Int. J. Heat Mass Tran.*, *10*, 567–580.
Gudmundsson, M. T. (2003), Melting of ice by magma-ice-water interactions during subglacial eruptions as an indicator of heat transfer in subaqueous eruptions, in *Explosive Subaqueous Volcanism*, *Geophys. Monogr. Ser.*, vol. 140, edited by J. D. L. White, J. L. Smellie, and D. A. Clague, pp 61–72, AGU, Washington, D. C., doi:10.1029/140GM04.
Gudmundsson, M. T. (2005), Subglacial volcanic activity in Iceland, in *Iceland: Modern Processes, Past Environments*, *Developments in Quaternary Science*, vol. 5, edited by C. J. Caseldine et al., pp. 127–151, Elsevier, Amsterdam.
Gudmundsson, M. T., F. Sigmundsson, and H. Bjornsson (1997), Ice–volcano interaction of the 1996 Gjálp subglacial eruption, Vatnajökull, Iceland, *Nature*, *389*, 954–957.
Gudmundsson, M. T., F. Sigmundsson, H. Bjornsson, and T. Hognadottir (2004), The 1996 eruption at Gjálp, Vatnajökull ice cap, Iceland: efficiency of heat transfer, ice deformation and subglacial water pressure, *Bull. Volcanol.*, *66*, 46–65.
Herranz, L. E., M. H. Anderson, and M. L. Corradini (1998), A diffusion layer model for steam condensation within the AP600 containment, *Nucl. Eng. Des.*, *183*, 133–150.
Höskuldsson, A., and R. S. J. Sparks (1997), Thermodynamics and fluid dynamics of effusive subglacial eruptions, *Bull. Volcanol.*, *59*, 219–230.
Huhtiniemi, I. K., and M. L. Corradini (1993), Condensation in the presence of noncondensable gases, *Nucl. Eng. Des.*, *141*, 429–446.
Incropera, F. P., and D. P. DeWitt (1996), *Introduction to Heat Transfer*, John Wiley, New York.
Kay, J. M., and R. M. Nedderman (1985), *Fluid Mechanics and Transfer Processes*, Cambridge Univ. Press, Cambridge, U. K.
Kim, J.-W., Y.-G. Lee, H.-K. Ahn, and G.-C. Park (2009), Condensation heat transfer characteristic in the presence of noncondensable gas on natural convection at high pressure, *Nucl. Eng. Des.*, *239*, 688–698.
Kim, M. H., and M. L. Corradini (1990), Modelling of condensation heat transfer in a reactor containment, *Nucl. Eng. Des.*, *118*, 193–212.
Magnússon, E., M. T. Gudmundsson, G. Sigurdsson, M. J. Roberts, F. Höskuldsson, and B. Oddsson (2012), Ice-volcano interactions during the 2010 Eyjafjallajökull eruption, as revealed by airborne radar, *J. Geophys. Res.*, *117*, B07405, doi:10.1029/2012JB009250.
Martinerie, P., D. Raynaud, D. M. Etheridge, J.-M. Barnola, and D. Mazaudier (1992), Physical and climatic parameters which influence the air content in polar ice, *Earth Planet. Sci. Lett.*, *112*, 1–13.
Marto, P. J. (1998), Condensation, in *Handbook of Heat Transfer*, 3rd ed., edited by W. M. Rohsenow, J. P. Hartnett, and Y. I. Cho, pp. 14.1–14.63, McGraw Hill, New York.
Massey, B. S. (1970), *Mechanics of Fluids*, Van Nostrand Reinhold, London.
Minkowycz, W., and E. Sparrow (1966), Condensation heat transfer in the presence of noncondensables, interfacial resistance, superheating, variable properties and diffusion, *Int. J. Heat Mass Tran.*, *9*, 1125–1144.
Ozbelge, T. A. (2001), Heat transfer enhancement in turbulent upward flows of liquid-solid suspensions through vertical annuli, *Int. J. Heat Mass Tran.*, *44*, 3373–3379.
Piriz, A. R., O. D. Cortazar, and J. J. Lopez Cela (2006), The Rayleigh-Taylor instability, *Am. J. Phys.*, *74*, 1095–1098.
Raithby, G. D., and K. G. T. Hollands (1998), Natural convection, in *Handbook of Heat Transfer*, 3rd ed., edited by W. M. Rohsenow, J. P. Hartnett, and Y. I. Cho, pp. 4.1–4.99, McGraw Hill, New York.
Rogers, G. F. C., and Y. R. Mayhew (1980), *Thermodynamic and Transport Properties of Fluids*, Blackwell, Oxford, U. K.
Rose, J. W. (1998), Condensation heat transfer fundamentals, *Trans. Inst. Chem. Eng.*, *76*, 143–152.
Sigvaldson, G. E., and G. Elisson (1968), Collection and analysis of volcanic gases at Surtsey, Iceland, *Geochim. Cosmochim. Acta*, *32*, 797–805.
Smellie, J. L. (2002), The 1969 subglacial eruption on Deception Island (Antarctica): Events and processes during an eruption beneath a thin glacier and implications for volcanic hazards, *Geol. Soc. London Spec. Publ.*, *202*, 59–79.
Sparrow, E. M., W. J. Minkowycz, and M. Saddy (1967), Forced convection in the presence of noncondensables and interfacial resistance, *Int. J. Heat Mass Tran.*, *10*, 1829–1845.
Tuffen, H. (2007), Models of ice melting and edifice growth at the onset of subglacial basaltic eruptions, *J. Geophys. Res.*, *112*, B03203, doi:10.1029/2006JB004523.

Tuffen, H., H. Pinkerton, D. W. McGarvie, and J. S. Gilbert (2002), Melting of the glacier base during a small-volume subglacial rhyolite eruption: Evidence from Blahnukur, Iceland, *Sediment. Geol.*, *149*, 183–198.
Turner, J. S. (1973), *Buoyancy Effects in Fluids*, Cambridge Univ. Press, Cambridge, U. K.
Wallace, P., and A. T. Anderson (2000), Volatiles in magmas, in *Encyclopedia of Volcanoes*, edited by H. Sigurdsson, Academic Press, San Diego, Calif.
Wilson, L., and J. W. Head (2002), Heat transfer and melting in subglacial basaltic volcanic eruptions: Implications for volcanic deposit morphology and meltwater volumes, *Geol. Soc. Spec. Publ.*, *202*, 59–79.
Wilson, L., and J. W. Head (2007), Heat transfer in volcano-ice interactions on Earth, *Ann. Glaciol.*, *45*, 83–86.
Woodcock, D. C., S. J. Lane, and J. S. Gilbert (2014), Ice-melt rates in liquid-filled cavities during explosive subglacial eruptions, *J. Geophys. Res. Solid Earth*, *119*, 1803–1817, doi:10.1002/2013JB010617.
Yen, Y.-C., A. Zehnder, S. Zavoluk, and C. Tien (1973), Condensation-melting heat transfer in the presence of air, *AIChE Symp. Ser.*, vol. 131(69), 23–29.